Journal of Fluorine Chemistry 131 (2010) 467–476

Contents lists available at ScienceDirect

Journal of Fluorine Chemistry

journal homepage: www.elsevier.com/locate/fluor

NMR spectral enantioresolution of spirobrassinin and 1-methoxyspirobrassinin enantiomers using (*S*)-(−)-ethyl lactate and modeling of spirobrassinin self-association for rationalization of its self-induced diastereomeric anisochromism (SIDA) and enantiomer self-disproportionation on achiral-phase chromatography (ESDAC) phenomena

Karel D. Klika [a,*], Mariana Budovská [a,b], Peter Kutschy [b]

[a] *Department of Chemistry, University of Turku, Vatselankatu 2, FIN-20014 Turku, Finland*
[b] *Institute of Chemical Sciences, Faculty of Science, P.J. Šafárik University, Moyzesova 11, 040 01 Košice, Slovak Republic*

ARTICLE INFO

Article history:
Received 30 September 2009
Received in revised form 26 October 2009
Accepted 30 October 2009
Available online 12 November 2009

Keywords:
Spirobrassinin
NMR
Enantiodifferentiation
DFT calculations
Self-disproportionation of enantiomers

ABSTRACT

The phytoalexin spirobrassinin is known to exhibit the unusual phenomenon of enantiomer self-disproportionation on achiral-phase chromatography (ESDAC) whereby the enantiomeric composition of a non-racemic mixture varies across the eluting chromatographic peak. However, spirobrassinin is exceptional since both early and late fractions are enantioenriched in comparison to the starting enantiomeric composition. This behavior is rationalized by the formation of two different complexes, substantiated by DFT calculations at the B3LYP/TZVP level of theory, both of which are in dynamic equilibrium with the free molecules. Concomitant with complexation under chromatographic conditions, complexation was also evident by NMR including the observation of distinct NMR signals for each enantiomer for some spins in a non-racemic mixture—the phenomenon of self-induced diastereomeric anisochromism (SIDA). Enantioresolution of various ^{1}H, ^{13}C and ^{15}N NMR signals were also induced for the enantiomers of spirobrassinin and another phytoalexin, 1-methoxyspirobrassinin, by application of the chiral solvating agent (*S*)-(−)-ethyl lactate, a cheap reagent with potentially broad applications. For spirobrassinin, the observed NMR signals were evaluated against values calculated using the GIAO method at the B3LYP/cc-pVTZ level of theory.

1. Introduction

Phytoalexins are structurally diverse, low molecular weight, and generally lipophilic substances possessing antimicrobial properties that are formed by plants in response to pathogenic attack or physical or chemical stress, probably as a result of the de novo synthesis of enzymes [1]. A particular group of these stress metabolites, the cruciferous phytoalexins, are specifically produced [2,3] by economically important members of the *Cruciferae* family including notable examples such as cabbage, turnip, Chinese cabbage, Japanese radish, wasabi, broccoli, rapeseed and arabidopsis, amongst others. A structural feature common to the more than 40 hitherto isolated cruciferous phytoalexins is the presence of an indole or indole-related nucleus possessing either a side chain or affixed to another heterocycle with either additional moiety containing one or two sulfur atoms [3]. In addition to their antimicrobial effects, cruciferous phytoalexins also exhibit anticancer activity against both human and animal cancers [4–8] and thus they are interesting lead compounds for anticancer drug development [9]. Cruciferous phytoalexins are also interesting from a structural perspective since those with a dihydrothiazole ring spiro-attached to the 3 position of the indole ring express chirality.

Since enantiomers of a chiral drug may, and often do, exhibit divergent pharmaceutical properties [10], evaluation of drug stereochemistry with respect to pharmacokinetics and pharmaceutical activity is consequently vital and, moreover, enantiomeric composition [11] determination of such drugs is deemed essential by many regulatory authorities. HPLC using chiral stationary phases is the most widely used technique for the determination of enantiomeric composition [12], although NMR employing chiral solvating agents (CSA) is also widespread [13]. In the latter case, the transient diastereomeric adducts formed between a CSA and the two enantiomers of the chiral analyte can potentially give rise to anisochronous NMR resonances, in which case the enantiomeric composition can be readily assessed directly from the NMR

* Corresponding author. Tel.: +358 2 3336826; fax: +358 2 3336700.
E-mail address: klikakd@yahoo.co.uk (K.D. Klika).

0022-1139/$ – see front matter © 2009 Elsevier B.V. All rights reserved.
doi:10.1016/j.jfluchem.2009.10.018

spectrum. However, absolute configuration determination of analytes a priori nonetheless is a challenge and remains far from routine [13].

Interestingly, a CSA is not always requisite for the observation of distinct NMR resonances for chiral analytes in cases of non-racemic mixtures as the self-association of suitable analytes under NMR conditions can lead to distinct NMR signals for the two enantiomers. This phenomenon of self-induced diastereomeric anisochromism (SIDA), though seemingly uncommon, is well-documented (e.g. Ref. [14] lists, in addition to its own example, some 36 cases). Related to SIDA is the phenomenon of enantiomer self-disproportionation on achiral-phase chromatography (ESDAC) whereby the enantiomeric composition of a non-racemic mixture varies across the eluting band in comparison to the initial enantiomeric composition of the sample that was loaded onto the column. In common with SIDA, ESDAC too is considered to arise from the formation of complexes [14,15], though the phenomenon is less-appreciated and less common in reported terms with only some 17 described [16] unique accounts together with a further 12 treatments [14,17].

Amongst the cruciferous phytoalexins, several spiroindoline[3,5′]thiazolidine-type phytoalexins have been described including (*S*)-(−)-spirobrassinin (**1**$_{\mathbf{S}}$), which was isolated [18] in 1987 from *Pseudomonas cichorii*-inoculated Japanese radish 'Daikon' (*Raphanus sativus*). The absolute configuration of (*S*)-(−)-spirobrassinin (**1**$_{\mathbf{S}}$) was determined [19] by X-ray crystallographic analysis after preparation of racemic (±)-spirobrassinin (**1**$_{\mathbf{rac}}$) by the cyclization of racemic (±)-dioxibrassinin with either $SOCl_2$ or MsCl followed by enantioresolution using (*S*)-(−)-1-phenylethyl isothiocyanate to obtain the pure enantiomer. Another spiroindoline[3,5′]thiazolidine-type phytoalexin, (*R*)-(+)-1-methoxyspirobrassinin (**2**$_{\mathbf{R}}$), was isolated [20] in 1994 from kohlrabi (*Brassica oleracea* var. *gongylodes*) after elicitation by UV radiation. The synthesis of racemic (±)-1-methoxyspirobrassinin (**2**$_{\mathbf{rac}}$) was accomplished by the dioxane–dibromide-mediated spirocyclization of 1-methoxybrassinin [21] whilst the stereoselective synthesis of naturally occurring (*R*)-(+)-1-methoxyspirobrassinin (**2**$_{\mathbf{R}}$) [22] and its absolute configuration determination have only been described recently [23].

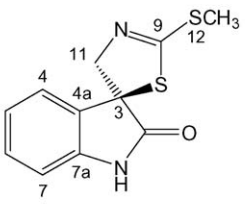

(*S*)-(-)-spirobrassinin (**1**$_{\mathbf{S}}$)

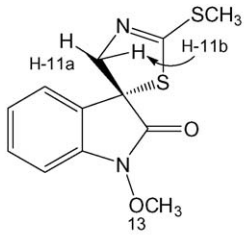

(*R*)-(+)-methoxyspirobrassinin (**2**$_{\mathbf{R}}$)

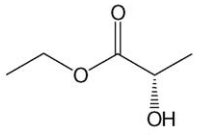

(*S*)-(-)-ethyl lactate (**3**$_{\mathbf{S}}$)

Previously, Pedras et al. have reported [24] a simple method for the ^{1}H NMR spectroscopic enantioresolution of **1**$_{\mathbf{rac}}$, **2**$_{\mathbf{rac}}$ and the synthetic analog 1-methylspirobrassinin using 2,2,2-trifluoro-1-(9-anthryl)ethanol (Pirkle's alcohol) as the CSA in C_6D_6. Although Pirkle's alcohol can cost upwards of ca. $350/g, the method is nonetheless relatively inexpensive on a cost per analysis basis if used routinely. However, we sought an alternative for modeling-based reasons and to this end examined (*S*)-(−)-ethyl lactate (**3**$_{\mathbf{S}}$) wherein it was found to resolve both racemic (±)-spirobrassinin (**1**$_{\mathbf{rac}}$) and racemic (±)-1-methoxyspirobrassinin (**2**$_{\mathbf{rac}}$) to a sufficient degree whereby it is amenable for practical application. And at ca. $0.03/g, it is considerably more affordable for trial resolutions. Additionally, we also examined the behavior of **1** with respect to both the SIDA and ESDAC phenomena. Compound **1** is exceptional insofar that it, together with its 8-oxo analog, represents the only examples [19] of compounds exhibiting "double ESDAC" whereby two elevations of the enantiomeric composition are observed across a chromatographic peak, i.e. both early and late fractions are enantioenriched in comparison to the initial enantiomeric composition. We also desired a deeper appreciation of the CSA–analyte interactions, as well as between the analytes themselves, in order to be able to not only predict successful spectroscopic and/or chromatographic resolution, but to also be able to determine the configuration of the analytes. Thus, the geometries and energies of the diastereomeric complexes were evaluated by DFT calculations at the B3LYP/TZVP level of theory in a similar fashion to previous works [14,15,25] in order to rationalize the spectroscopic observations and chromatographic behavior. Reliable prediction of the NMR data by calculating the shieldings of the complexes formed between **3**$_{\mathbf{S}}$ and the spirobrassinin enantiomers – **1**$_{\mathbf{S}}$·**3**$_{\mathbf{S}}$ and **1**$_{\mathbf{R}}$·**3**$_{\mathbf{S}}$ – using the GIAO method at the B3LYP/cc-pVTZ level of theory was also evaluated.

2. Experimental

2.1. Sample preparation

Racemic (±)-spirobrassinin (**1**$_{\mathbf{rac}}$) and both enantiomers **1**$_{\mathbf{R}}$ and **1**$_{\mathbf{S}}$ were prepared according to synthetic procedures to be published elsewhere with physical characteristics in accordance with literature values [3,18,19]. Racemic (±)-spirobrassinin (**1**$_{\mathbf{rac}}$): ^{1}H NMR (500 MHz, C_6D_6): δ 2.159 (3H, s, H-12), 4.183 (1H, d, J_{H11b} = −15.23 Hz, H-11a, proximal to the aromatic ring), 4.617 (1H, d, J_{H11a} = −15.23 Hz, H-11b, distal to the aromatic ring), 6.165 (1H, ddd, J_{H6} = 7.80, J_{H5} = 1.01, J_{H4} = 0.59 Hz, H-7), 6.657 (1H, td, J_{H6} = 7.67, J_{H4} = 7.54, J_{H7} = 1.01 Hz, H-5), 6.813 (1H, td, J_{H7} = 7.80, J_{H5} = 7.67, J_{H4} = 1.25 Hz, H-6), 6.997 (1H, ddt, J_{H5} = 7.54, J_{H6} = 1.25, J_{H7} = 0.59, J_{H1} = 0.69 Hz, H-4), 7.378 (1H, bs, J_{H4} unresolved, NH). ^{13}C NMR (125 MHz, C_6D_6): δ 15.28 (C-12), 65.04 (C-3), 75.21 (C-11), 110.06 (C-7), 123.27 (C-5), 124.57 (C-4), 129.35 (C-6), 131.78 (C-4a), 140.22 (C-7a), 163.27 (C-9), 177.45 (C-2). ^{15}N NMR (60 MHz, C_6D_6): δ −249.98 (N-1), −97.4 (N-10).

Racemic (±)-1-methoxyspirobrassinin (**2**$_{\mathbf{rac}}$) was synthesized as previously described [21] and similarly for the synthesis of both enantiomers **2**$_{\mathbf{R}}$ and **2**$_{\mathbf{S}}$ [22] with physical characteristics in accordance with reported literature values. Racemic (±)-1-methoxyspirobrassinin (**2**$_{\mathbf{rac}}$): ^{1}H NMR (500 MHz, C_6D_6): δ 2.146 (3H, s, H-12), 3.428 (3H, s, H-13), 4.065 (1H, d, J_{H11b} = −15.36 Hz, H-11a, proximal to the aromatic ring), 4.530 (1H, d, J_{H11a} = −15.36 Hz, H-11b, distal to the aromatic ring), 6.538 (1H, ddd, J_{H6} = 7.79, J_{H5} = 1.04, J_{H4} = 0.59 Hz, H-7), 6.676 (1H, td, J_{H6} = 7.70, J_{H4} = 7.51, J_{H7} = 1.04 Hz, H-5), 6.883 (1H, td, J_{H7} = 7.79, J_{H5} = 7.70, J_{H4} = 1.17 Hz, H-6), 6.967 (1H, ddd, J_{H5} = 7.51, J_{H6} = 1.17, J_{H7} = 0.59 Hz, H-4). ^{13}C NMR (125 MHz, C_6D_6): δ 15.28 (C-12), 63.16 (C-13), 63.24 (C-3), 74.70 (C-11), 107.60 (C-7), 123.86 (C-5), 124.50 (C-4), 129.62 (C-6), 127.62 (C-4a), 139.93 (C-7a), 163.06 (C-9), 170.68 (C-2). ^{15}N NMR (60 MHz, C_6D_6): δ −184.6 (N-1), −97.33 (N-10).

2.2. NMR methods

NMR spectra were acquired on Bruker Avance NMR spectrometers at 500, 125 and 60 MHz for ^{1}H, ^{13}C and ^{15}N nuclei, respectively, at 25 °C unless specified otherwise. Samples of

spirobrassinin (**1**) and 1-methoxyspirobrassinin (**2**) for NMR measurements consisted of concentrated samples (ca. 20 mg in 0.6–0.7 mL of C_6D_6) or dilute samples (ca. 5 mg in 0.6–0.7 mL of C_6D_6) and were prepared from racemic mixtures or non-racemic mixtures [11] in the case of **1** (e.g. $\mathbf{1_R}$:$\mathbf{1_S}$, 64.2:35.8). For enantioresolution using $\mathbf{3_S}$, portions of $\mathbf{3_S}$ were added directly to the NMR samples of spirobrassinin (**1**) and 1-methoxyspirobrassinin (**2**). For assignment purposes, a standard set of correlation experiments {DQF-COSY, COSY-45 (for the signs of $^2J_{H11a,H11b}$), HSQC, HMBC and 1D-NOESY [26]} were applied; full experimental details for all NMR experiments have been described elsewhere [27,28]. For ^{15}N chemical shift measurements, resonances were observed directly (with values being reported to two decimal places) for concentrated samples and for nitrogen atoms with a directly bound proton using, as appropriate, DEPT optimized for a $^1J_{H,N}$ coupling of 90 Hz and INEPT optimized for a $^nJ_{H,N}$ coupling of 4.1 Hz; for other cases, the resonances were observed indirectly (with these indirect values being reported to only one decimal place) using HMBC with $^nJ_{H,N}$ optimized for 8.0 or 4.1 Hz. The selection of 4.1 Hz was made based on the measurement of the coupling $^2J_{H11a,N10}$ taken from a 1D HMBC spectrum. The chemical shifts of ^{1}H and ^{13}C nuclei are reported relative to TMS incorporated as an internal standard (0 ppm for both nuclei) whilst the chemical shifts of ^{15}N nuclei are reported relative to nitromethane (0 ppm) measured externally. Spin analysis was performed using *Perch* iteration software [29] for the precise extraction of ^{1}H chemical shifts and $J_{H,H}$ coupling constants whilst the deconvolution subroutine of the program was utilized for accurate quantification of overlapped signals.

2.3. Chromatographic experiments

The HPLC chromatographic ESDAC results of reference [19] are utilized and referred to in the analysis (e.g. Fig. 5). Checks for perturbation of the enantiomeric composition either via complexation with $\mathbf{3_S}$ or via ESDAC under chromatographic conditions were made by either the addition of silica gel to the NMR sample (“TLC in an NMR tube”) or by “panning”. In the former case, by the addition of 25 or 50 mg allotments of silica gel to an NMR sample containing either ca. 2 mg of racemic (±)-spirobrassinin ($\mathbf{1_{rac}}$) and a 24-fold excess of $\mathbf{3_S}$ (total of 125 mg of silica gel) or, for observation of ESDAC, ca. 10 mg of non-racemic spirobrassinin ($\mathbf{1_R}$:$\mathbf{1_S}$, 64.2:35.8; total of 200 mg silica gel). In the latter case, “panning”, four pots containing ca. 100 mg of silica gel and 40 μL of $\mathbf{3_S}$ were used each laden with ca. 1 mL of toluene. A sample of non-racemic spirobrassinin ($\mathbf{1_R}$:$\mathbf{1_S}$, 64.2:35.8), ca. 4 mg in solution (1 mL) was then added to the first pot and the system allowed to equilibrate by swirling the pot for several minutes and leaving to stand. Following equilibration, the effluent was transferred to the next pot by Pasteur pipette. The process was repeated with the effluent being transferred from pot to pot sequentially after equilibration. Finally, after the fourth pot, analysis of the contents of the effluent with respect to enantiomeric composition was made.

2.4. Computational methods

DFT quantum chemical calculations were performed within the framework of the DFT method according to the original proposal [30] using the *Gaussian03* program [31] with a similar approach to previous studies [14,15,25]. Individual molecules were first free-hand formulated and then optimized following which the two parts of a particular complex were incorporated and positioned with appropriate orientation. Structures were calculated using the restricted B3LYP functional [30,32] with the following basis sets: 6-31G(d,p) (initial geometry optimizations and frequency calculations in the gas phase), TZVP (final geometry optimizations and frequency calculations with inclusion of benzene or water as the solvent) and cc-pVTZ (chemical shieldings on TZVP-optimized structures with inclusion of benzene as the solvent). Solvents were simulated by IEF-PCM using the uahf atomic radii set. Optimizations utilized the keyword gdiis option for the convergence algorithm. Frequency calculations using the keyword noraman option were also conducted on the final structures to confirm that they were true minima on the potential energy surface by not providing imaginary frequencies above 100 cm^{-1} (instances of imaginary frequencies are listed in Supplementary Data) and to obtain the thermodynamic contributions at 298.15 K (wherein calculated frequencies were scaled by a factor of 0.9806 [33]). Absolute shieldings were calculated using the GIAO method [34]. Figures of optimized structures and associated Cartesian coordinates are presented in Supplementary Data.

3. Results and discussion

3.1. Conformational analysis of $\mathbf{1}_{rac}$ and $\mathbf{2}_{rac}$ with $\mathbf{3_S}$

Initial examinations of spirobrassinin (**1**) at the B3LYP/6-31G(d,p) level of theory in the gas phase of freely drawn structures yielded only two stable conformations (see Supplementary Data) for **1**. Whilst the pyrrolidinone ring was determined to be essentially flat, the dihydrothiazole ring adopted an envelope conformation with C-3 as the out-of-plane atom. However, of the two possible envelope conformations given the restrictions of the N_{10}=C_9 imine double bond, only one was found to be stable with the alternate conformation realizing the more stable arrangement during optimization. The –SCH_3 group could be orientated either directly towards the imine nitrogen N-10 or orientated away from the imine nitrogen N-10 to provide the two conformations with the former being preferred over the latter by 2.33 kcal/mol. Since similar energetic conformational preferences were found under complexation either via the amide group or via the imine nitrogen N-10 to $\mathbf{3_S}$ under similar computational conditions, only the most stable conformation was utilized for subsequent computations at the higher level under solvetic conditions for both complexation to $\mathbf{3_S}$ and the dimeric complexation of **1**.

3.2. Self-induced diastereomeric anisochromism (SIDA)

The SIDA phenomenon has not been reported for spirobrassinin (**1**) previously but its occurrence was strongly anticipated since ESDAC and SIDA commonly involve the formation of dimeric complexes [14,15]. The occurrence of SIDA was evaluated by examination of a non-racemic mixture of $\mathbf{1_R}$ and $\mathbf{1_S}$ (64.2:35.8, respectively) in C_6D_6 and for which distinct NMR signals were observed for the two enantiomers for a number of ^{1}H, ^{13}C and ^{15}N resonances. For the ^{1}H signals, the largest chemical shift difference ($\Delta\delta$) was observed for the NH proton H-1 ($\Delta\delta$, −19.85 ppb) whilst the largest ^{13}C $\Delta\delta$s were for the carbonyl C-2 ($\Delta\delta$, −25.05 ppb) and the imine C-9 ($\Delta\delta$, 23.00 ppb) signals. Both amide N-1 and imine N-10 signals were strongly differentiated ($\Delta\delta$s, −44.65 and −15.20 ppb, respectively). Differentiation for most of the signals were accentuated by acquisition at 5 °C whilst conversely, enantioresolution was severely attenuated upon dilution wherein the spectra obtained were essentially indistinguishable [35] from that for the racemic mixture at similar concentration. Results for all ^{1}H, ^{13}C and ^{15}N signals are listed in Tables 1 and 2 whilst various example signals exhibiting SIDA are shown in Figs. 1 and 2. The very observation of SIDA in itself for **1** effectively proves the self-association of the molecule and thereby implicates the formation of dimeric complexes.

The SIDA phenomenon was also evaluated by modeling hydrogen bonded homo- and heterochiral dimeric self-associations of

Table 1
^{1}H NMR chemical shift inequalities caused by SIDA for the enantiomers of a non-racemic mixture of spirobrassinin (**1**$_{R}$:**1**$_{S}$, 64.2:35.8).

Sample	[a]	H-1	H-4	H-5	H-6	H-7	H-11a	H-11b	H-12
Enrich. **1**$_{R}$, conc.	δ (ppm)[b]	8.644	7.010	6.671	6.826	6.330	4.197	4.622	2.166
	$\Delta\delta$ (ppb)	−19.850	–	–	0.839	na	−2.040	1.812	−0.496
	$\Delta\nu$ (Hz)	−9.928	–	–	0.420	na	−1.020	0.906	−0.248
Enrich. **1**$_{R}$, conc.[c]	δ (ppm)[b]	9.333	6.982	6.656	6.813	6.377	4.164	4.601	2.129
	$\Delta\delta$ (ppb)	−18.706	na	–	2.155	na	−4.138	1.754	−0.744
	$\Delta\nu$ (Hz)	−9.356	na	–	1.078	na	−2.069	0.877	−0.372
Enrich. **1**$_{R}$, dilute	δ (ppm)[b]	7.312	6.996	6.655	6.811	6.152	4.181	4.616	2.158
	$\Delta\delta$ (ppb)	−12.375	–	–	–	na	−0.972	0.877	–
	$\Delta\nu$ (Hz)	−6.189	–	–	–	na	−0.486	0.439	–
1$_{rac}$, dilute	δ (ppm)	7.378	6.997	6.657	6.813	6.165	4.183	4.617	2.159

na: splitting not assessed.
[a] The quantities $\Delta\delta$ and $\Delta\nu$ are the differences {value for the (*R*)-enantiomer − value for the (*S*)-enantiomer} between the signals of the two enantiomers in ppm and frequency, respectively.
[b] Chemical shifts of the signals of the (*R*)-enantiomer **1**$_{R}$.
[c] Spectrum acquired at 5 °C.

Table 2
^{13}C and ^{15}N NMR chemical shift inequalities caused by SIDA for the enantiomers of a non-racemic mixture of spirobrassinin (**1**$_{R}$:**1**$_{S}$, 64.2:35.8).

Sample	[a]	C-2	C-3	C-4	C-4a	C-5	C-6	C-7	C-7a	C-9	C-11	C-12	N-1	N-10
Enrich. **1**$_{R}$, conc.	δ (ppm)[b]	178.53	65.25	124.51	131.17	123.36	129.50	110.46	140.46	163.35	75.15	15.28	−247.99	−97.48
	$\Delta\delta$ (ppb)	−21.63	3.19	–	7.29	–	–	–	−4.10	20.27	4.55	–	−15.20	−44.65
	$\Delta\nu$ (Hz)	−2.721	0.401	–	0.916	–	–	–	−0.515	2.549	0.573	–	−0.925	−2.717
Enrich. **1**$_{R}$, conc.[c]	δ (ppm)[b]	179.07	65.24	124.47	130.87	123.36	129.55	110.63	140.55	163.31	74.96	15.28	nm	nm
	$\Delta\delta$ (ppb)	−25.05	6.83	–	11.39	–	–	–	–	23.00	4.55	–	–	–
	$\Delta\nu$ (Hz)	−3.150	0.859	–	1.432	–	–	–	–	2.893	0.573	–	–	–
Enrich. **1**$_{R}$, dilute	δ (ppm)[b]	177.41	65.03	124.57	131.36	123.27	129.34	110.04	140.20	163.26	75.21	15.27	−249.99	−97.4
	$\Delta\delta$ (ppb)	4.10	–	–	5.01	–	–	–	–	−11.61	–	–	−19.95	–
	$\Delta\nu$ (Hz)	0.515	–	–	0.630	–	–	–	–	−1.461	–	–	−1.214	–
1$_{rac}$, dilute	δ (ppm)	177.45	65.04	124.57	131.35	123.27	129.35	110.06	140.22	163.27	75.21	15.28	nm	nm

nm: not measured.
[a] The quantities $\Delta\delta$ and $\Delta\nu$ are the differences {value for the (*R*)-enantiomer − value for the (*S*)-enantiomer} between the signals of the two enantiomers in ppm and frequency, respectively.
[b] Chemical shifts of the signals of the (*R*)-enantiomer **1**$_{R}$.
[c] Spectrum acquired at 5 °C.

spirobrassinin (**1**). Two interactions were evaluated, bidentate amide-to-amide bound complexes (i.e. hydrogen bonds formed between the amide NH and the carbonyl oxygen) and monodentate amide-to-imine bound complexes (i.e. a hydrogen bond formed between the amide NH of one molecule and the imine nitrogen of another molecule). For amide-to-amide complexation, the homo- and heterochiral constructs, **1**$_{S}$·**1**$_{S}$ and **1**$_{R}$·**1**$_{S}$, respectively, were deemed to be rather rigid due to the bidentate complexation and the restricted flexibility of the molecular units themselves. Depictions of the amide-to-amide complexes **1**$_{S}$·**1**$_{S}$ and **1**$_{R}$·**1**$_{S}$ are shown in Fig. 3. For the monodentate amide-to-imine complexes, there was greater flexibility though only two conformers were evaluated, denoted as 1

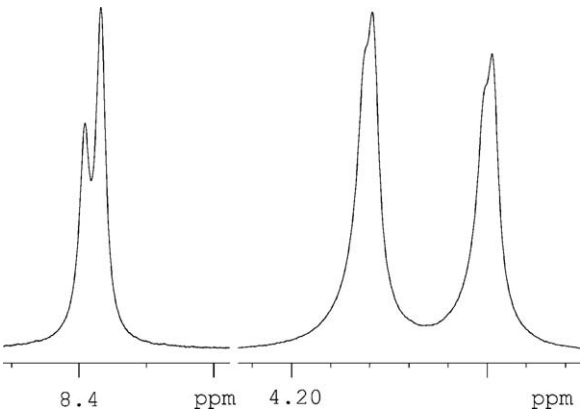

Fig. 1. SIDA-enantiodifferentiated proton signals for the amide H-1 singlet (left trace) and the H-11a doublet (right trace) of the spirobrassinin enantiomers **1**$_{R}$ and **1**$_{S}$ (64.2:35.8, respectively). The H-1 signal intensities, after deconvolution and in accordance with accredited SIDA behavior [14], correctly reflect the enantiomeric composition.

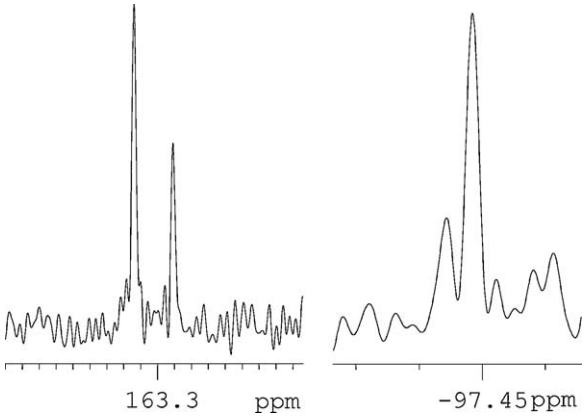

Fig. 2. SIDA-enantiodifferentiated signals for the imine carbon C-9 (left trace) and the imine nitrogen N-10 (right trace) of the spirobrassinin enantiomers **1**$_{R}$ and **1**$_{S}$ (64.2:35.8, respectively). For technical reasons, the ^{13}C and ^{15}N signals may not reflect the enantiomeric composition, as anticipated in accordance with accredited SIDA behavior [14].

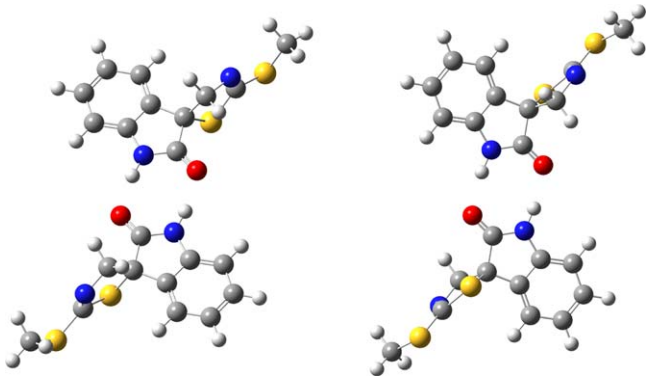

Fig. 3. The geometry-optimized structures of the amide-to-amide bound homochiral $\mathbf{1_S}\cdot\mathbf{1_S}$ (left) and heterochiral $\mathbf{1_R}\cdot\mathbf{1_S}$ (right) complexes at the B3LYP/TZVP (IEF-PCM) level of theory in benzene.

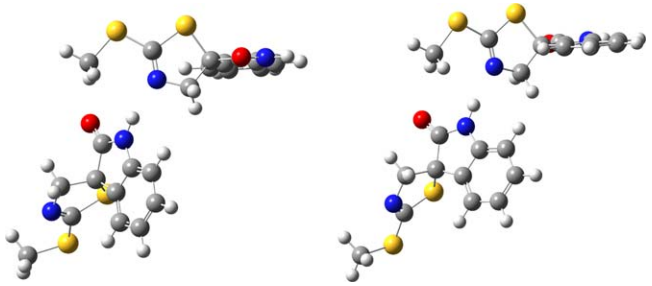

Fig. 4. The geometry-optimized structures of the amide-to-imine bound homochiral $\mathbf{1_S}\cdot\mathbf{1_S}$ (left) and heterochiral $\mathbf{1_R}\cdot\mathbf{1_S}$ (right) complexes at the B3LYP/TZVP (IEF-PCM) level of theory in benzene.

and 2, which differed by 180° rotation of one molecular unit relative to the other. Depictions of two of the amide-to-imine complexes $\mathbf{1_S}\cdot\mathbf{1_S}$ and $\mathbf{1_R}\cdot\mathbf{1_S}$ complexes are portrayed in Fig. 4 with further depictions of all structures presented in the Supplementary data.

The amide-to-amide complexes were calculated to be highly favored in energy over the amide-to-imine complexes by several kcal/mol in benzene (Table 3, vide infra). Within each mode, a homochiral complex was the more stable complex (for amide-to-amide complexes, ΔG, 0.28 kcal/mol; for amide-to-imine complexes, ΔG, 0.26 kcal/mol). Though the calculations imply total domination in solution by the amide-to-amide structures, experimentally there was considerable evidence for the presence of the amide-to-imine complexes in addition to the amide-to-amide complexes. For example, several NMR observations such as chemical shift changes (in comparison of dilute to concentrated samples), signal divergence between the two enantiomers and intermolecular NOEs. Though ^{15}N chemical shift changes due to protonation or hydrogen bonding can be difficult to predict and are oft counterintuitive, for the system examined here, hydrogen bonding should lead to shielding for the N-10 nitrogen [28,36] whilst for the N-1 amide nitrogen as a hydrogen bond donor, deshielding is anticipated [37] (this was also found computationally, vide infra). Minor shielding was in fact detected for N-1 (but by an amount below the level of reliability) whilst, and consistent with either mode, significant deshielding was observed for N-1. For all of the ^{1}H and ^{13}C nuclei, the observed chemical shift changes were consistent with either one or other mode or a combination thereof whilst unambiguous changes indicative of amide-to-imine complexation were lacking. However, the H-11a, H-11b, H12, C-9 and C-11 signals all exhibited SIDA and thereby were suggestive of amide-to-imine complexation. NOEs indicating amide-to-imine complexation included enhancements from H-11b to H-7 and the amide proton H-1. The latter interaction can potentially be, based on r_is taken from calculated structures, more than fourfold stronger than that to H-12 (–SCH_3). The actual observed ratio in a concentrated sample was ca. twofold, and furthermore, the H-11b/H-1 NOE was not measurable in a dilute solution. Also supporting amide-to-imine complexation was an NOE from H-1 to H-12.

Finally, the observation of "double ESDAC" (vide infra) conveys the insinuation that two distinct complexes must be participating in an equilibrium, albeit under chromatographic conditions. The source of the discrepancy between the experimental observations and theoretical calculations with regards to relative stabilities can only be attributed to various specific solute–solvent interactions such as π-stacking by the benzene molecules. It is also worth noting, however, that tautomeric equilibria can be notoriously difficult to predict accurately in terms of their energies, and particularly so when hydrogen bonding is involved [28,38].

3.3. Enantiomer self-disproportionation on achiral-phase chromatography (ESDAC)

Not only has a proficient ESDAC effect been observed for non-racemic mixtures of **1**, but the compound (and also its 8-oxo analog) is highly exceptional in that it exhibits [19] two elevations of the enantiomeric composition across a chromatographic band, i.e. a "double ESDAC" is, in essence, in effect. This highly unique behavior can be rationalized by the formation of two distinct complexes, viz. the amide-to-amide and amide-to-imine structures formulated in the previous section, both of which are in

Table 3
DFT-calculated electronic and Gibbs' free energies of homo- and heterochiral dimeric self-associations of the spirobrassinin enantiomers $\mathbf{1_R}$ and $\mathbf{1_S}$ at the B3LYP/TZVP (IEF-PCM) level of theory.

Structure	Complexation mode, amide-to-	Conform.	Solvent	ΔE (kcal/mol)	ΔG (kcal/mol)	Hydrogen bonds, r (Å)	
						N–H···N=C	C=O···H–N
$\mathbf{1_S}\cdot\mathbf{1_S}$	Amide	–	Benzene	0.06	0.00	1.864[a]	1.864
$\mathbf{1_R}\cdot\mathbf{1_S}$	Amide	–	Benzene	0.00	0.28	1.863[a]	1.865
$\mathbf{1_S}\cdot\mathbf{1_S}$	Imine	1	Benzene	6.56	5.94	2.011	–
$\mathbf{1_S}\cdot\mathbf{1_S}$	Imine	2	Benzene	6.92	7.35	2.004	–
$\mathbf{1_R}\cdot\mathbf{1_S}$	Imine	1	Benzene	7.03	6.20	2.006	–
$\mathbf{1_R}\cdot\mathbf{1_S}$	Imine	2	Benzene	6.56	6.26	2.015	–
$\mathbf{1_S}\cdot\mathbf{1_S}$	Amide	–	Water	0.13	0.08	1.883[a]	1.884
$\mathbf{1_R}\cdot\mathbf{1_S}$	Amide	–	Water	0.00	0.00	1.884[a]	1.883
$\mathbf{1_S}\cdot\mathbf{1_S}$	Imine	1	Water	2.25	2.65	2.004	–
$\mathbf{1_S}\cdot\mathbf{1_S}$	Imine	2	Water	2.27	2.24	1.995	–
$\mathbf{1_R}\cdot\mathbf{1_S}$	Imine	1	Water	2.36	2.11	1.987	–
$\mathbf{1_R}\cdot\mathbf{1_S}$	Imine	2	Water	2.23	0.93	2.010	–

[a] Hydrogen bond C=O···H–N.

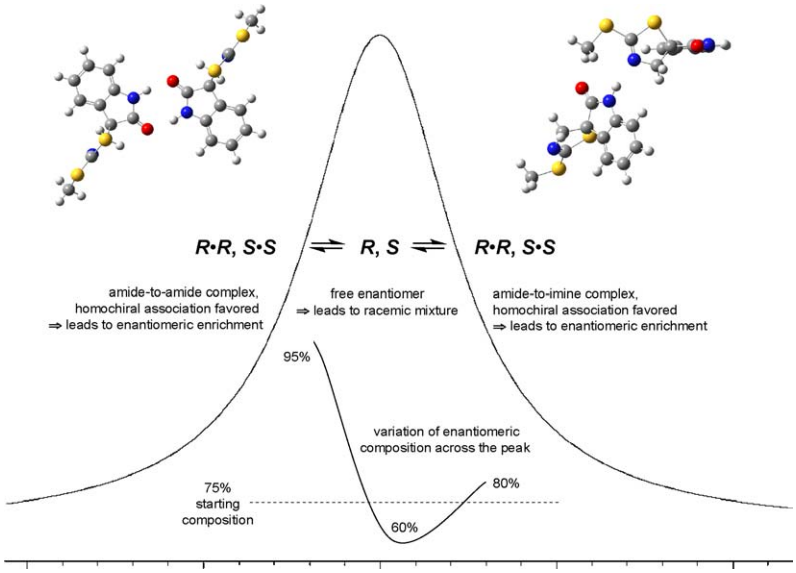

Fig. 5. Variation of the enantiomeric composition for a non-racemic sample of spirobrassinin (e.g. 75:25) across an eluting chromatographic peak due to different complexation modes. A typical composition trace [19] is depicted showing the early and late elevations of the enantiomer composition.

dynamic equilibrium with the free molecules during passage along the chromatographic column.

The energies of the homo- and heterochiral complexes in polar and non-polar environments (water and benzene, respectively) are presented in Table 3. The amide-to-imine complexes of **1** are more stabilized than the amide-to-amide complexes within a polar environment in comparison to a non-polar environment and hence they should be retarded under normal-phase chromatographic conditions relative to the progress of their counterparts. Since for both complexes in benzene it is the homochiral complex that is more energetically favored (thereby leading to enrichment of the predominant enantiomer for the relevant portion of the eluting peak), a plausible scenario that successfully explains the "double ESDAC" event is that the amide-to-amide complex elutes first, followed by the free enantiomers, then finally by the amide-to-imine complex, with both complexes in dynamic equilibrium with the single molecules. Thus, both early and late fractions of the chromatographic peak will be enantioenriched relative to the sample loaded onto the column whilst the middle of the peak will tend towards a racemic mixture. This process is portrayed graphically in Fig. 5.

Perturbation of the enantiomeric composition of a non-racemic mixture of $\mathbf{1_R}$ and $\mathbf{1_S}$ (64.2:35.8, respectively) in solution by the addition of silica gel to an NMR sample ("TLC in an NMR tube"), thus trying to elicit the ESDAC effect, was attempted but unequivocal results were not forthcoming despite the proficient ESDAC effect reported for **1** [19]. Though some, albeit very slight, discrimination was discernible, it bordered on the limits of reliable interpretation. Nonetheless, the perceived bias was towards $\mathbf{1_R}$ in concert with ESDAC observations. However, with the amide-to-amide and amide-to-imine structures both favoring the homochiral complex and thus both favoring enantioenrichment, under conditions of thermodynamic equilibrium the two tendencies oppose each other since one complex is more stabilized in one environment than the other. Hence the lack of observation of any perturbation from the original enantiomeric ratio under these conditions can be construed as being consistent with the calculations. Chromatographically it is likely that thermodynamic factors alone are not significant for the ESDAC effect in this instance thus alluding to the influence of kinetic factors.

3.4. Spectroscopic enantioresolution of $\mathbf{1}_{rac}$ and $\mathbf{2}_{rac}$ with $\mathbf{3}_S$

The enantiodiscriminating capability of CSA $\mathbf{3_S}$ towards the spirobrassinin enantiomers $\mathbf{1_R}$ and $\mathbf{1_S}$ and 1-methoxyspirobrassinin enantiomers $\mathbf{2_R}$ and $\mathbf{2_S}$ was examined using ^{1}H, ^{13}C and ^{15}N NMR by the incremental addition of aliquots of $\mathbf{3_S}$ to a C_6D_6 solution of racemic or enantioenriched substrate until sufficient differentiation of various signals of the enantiomers had been attained. With only an eightfold excess of $\mathbf{3_S}$, distinction was not observed for the proton signals of racemic (±)-spirobrassinin ($\mathbf{1_{rac}}$), however, with 43.9 equivalents of $\mathbf{3_S}$, resolution was observed for the signals of H-11a, H-4 and H-7. Improved enantioresolution was attained by increasing the amount of $\mathbf{3_S}$ further to a total of 88.5 equivalents, and then even more by lowering the sample temperature to 8 °C wherein the largest $\Delta\delta$s were observed for H-7 ($\Delta\delta$, 7.704 ppb) and H-11a ($\Delta\delta$, −3.165 ppb). Table 4 lists the ^{1}H signals for **1** under various selected conditions together with the $\mathbf{3_S}$-enantioresolved signals of racemic (±)-1-methoxyspirobrassinin ($\mathbf{2_{rac}}$). By ^{13}C NMR, the greatest discriminations for **1** were for the imine C-9 ($\Delta\delta$, −35.53 ppb) and carbonyl C-2 ($\Delta\delta$, 10.02 ppb) signals, also at a reduced temperature (8 °C); for **2**, enantioresolution was observed only for the signals of the carbonyl C-2, imine C-9 and methoxy C-13 carbons. By ^{15}N NMR, enantioresolution for both **1** and **2** was evident for both the amide N-1 and imine N-10 nitrogens. Table 5 lists the ^{13}C and ^{15}N signals for **1** and **2** under various conditions.

Clearly enantioresolution proficiency is highly dependent on the concentration of the analyte as well as the ratio of the analyte to the CSA $\mathbf{3_S}$ with effectiveness readily attenuated upon dilution at a maintained ratio of analyte to CSA. Nonetheless, on a practical level it is straightforward to persist with the addition of $\mathbf{3_S}$ until sufficient discrimination has been attained, and certainly bearing in mind the cost of $\mathbf{3_S}$, this is a very affordable option. However, it is worth noting that caveats regarding assignment based peak order and the measurement conditions in effect should be heeded [39] as indeed some signals for this system were in fact observed to swap order depending on the prevailing conditions. The situation, though, is highly complicated in this system and comprehending the positional changes of some signals is not straightforward due to the multiple modes of self-association for **1** (hence a three-state equilibrium between the free molecules **1** and the **1**·**1** amide-to-amide and **1**·**1** amide-to-imine bound complexes for **1** prior to

Table 4
^{1}H NMR enantioresolution of the spirobrassinin enantiomers $\mathbf{1_R}$ and $\mathbf{1_S}$ and 1-methoxyspirobrassinin enantiomers $\mathbf{2_R}$ and $\mathbf{2_S}$ by complexation with $\mathbf{3_S}$.

Sample	[a]	H-1	H-4	H-5	H-6	H-7	H-11a	H-11b	H-12
$\mathbf{1_{rac}}$, dilute	δ (ppm)	7.378	6.997	6.657	6.813	6.165	4.183	4.617	2.159
$\mathbf{1_{rac}}$, dilute + 8.64 equiv. $\mathbf{3_S}$	δ (ppm)[b]	7.723	7.012	6.670	6.836	6.279	4.194	4.623	2.167
$\mathbf{1_{rac}}$, dilute + 43.9 equiv. $\mathbf{3_S}$	δ (ppm)[b]	8.646	7.052	6.709	6.903	6.574	4.231	4.639	2.196
	$\Delta\delta$ (ppb)	–	1.259	–	–	3.699	−1.011	–	–
	$\Delta\nu$ (Hz)	–	0.629	–	–	1.841	−0.505	–	–
$\mathbf{1_{rac}}$, dilute + 88.5 equiv. $\mathbf{3_S}$	δ (ppm)[b]	9.148	7.080	~6.74	6.950	~6.75	4.260	4.650	2.226
	$\Delta\delta$ (ppb)	–	na	−0.571	–	–	−2.020	1.220	−0.458
	$\Delta\nu$ (Hz)	–	na	−0.296	–	–	−1.030	0.610	−0.210
$\mathbf{1_{rac}}$, dilute + 88.5 equiv. $\mathbf{3_S}$[c]	δ (ppm)[b]	9.600	7.068	6.737	6.962	6.866	4.243	4.643	2.204
	$\Delta\delta$ (ppb)	–	na	−0.610	0.706	7.704	−3.165	0.629	−0.534
	$\Delta\nu$ (Hz)	–	na	−0.353	0.353	3.853	−1.564	0.315	−0.257
Enrich. $\mathbf{1_R}$, conc. + 8.17 equiv. $\mathbf{3_S}$	δ (ppm)[b]	9.579	7.085	6.755	6.965	6.817	4.268	4.650	2.238
	$\Delta\delta$ (ppb)	–	na	−0.648	–	4.901	−3.661	1.392	−0.725
	$\Delta\nu$ (Hz)	–	na	−0.334	–	2.451	−1.831	0.696	−0.362
$\mathbf{2_{rac}}$, dilute	δ (ppm)	3.428[d]	6.967	6.676	6.883	6.538	4.065	4.530	2.146
$\mathbf{2_{rac}}$, dilute + 30.6 equiv. $\mathbf{3_S}$	δ (ppm)[e]	3.526[d]	7.025	6.746	6.960	6.608	4.146	4.572	2.223
	$\Delta\delta$ (ppb)	1.125	1.239	0.534	–	–	0.648	2.384	2.222
	$\Delta\nu$ (Hz)	0.553	0.62	0.267	–	–	0.324	1.202	0.477
$\mathbf{2_{rac}}$, conc. + 9.84 equiv. $\mathbf{3_S}$	δ (ppm)[e]	3.536[d]	7.027	6.754	6.970	6.619	4.150	4.570	2.230
	$\Delta\delta$ (ppb)	0.935	1.373	–	–	–	–	2.345	0.725
	$\Delta\nu$ (Hz)	0.477	0.687	–	–	–	–	1.173	0.362
$\mathbf{1_R}$·$\mathbf{3_S}$ − $\mathbf{1_R}$[f] (calculated[g])	$\Delta\delta$ (ppm)	−4.409	0.029	−0.002	−0.029	−0.219	0.020	0.012	0.005
$\mathbf{1_S}$·$\mathbf{3_S}$ − $\mathbf{1_R}$·$\mathbf{3_S}$[f] (calculated[g])	$\Delta\delta$ (ppm)	−0.253	−0.016	0.004	0.006	0.012	−0.023	−0.031	−0.006

na: splitting not assessed.
[a] The quantities $\Delta\delta$ and $\Delta\nu$ are the differences {value for the (*R*)-enantiomer − value for the (*S*)-enantiomer when known} between the signals of the two enantiomers in ppm and frequency, respectively.
[b] Chemical shifts of the signals of the (*R*)-enantiomer $\mathbf{1_R}$.
[c] Spectrum acquired at 8 °C.
[d] H-13.
[e] Enantiomers not identified.
[f] Difference of the shieldings, therefore negative values indicate that the former spin is deshielded relative to the latter.
[g] By DFT at the B3LYP/TZVP//B3LYP/cc-pVTZ level of theory using the GIAO method with solvation by benzene simulated by IEF-PCM using the uahf atomic radii set.

addition of the CSA) in addition to the multiple modes of binding to $\mathbf{3_S}$ further compounding the situation. However, the ^{1}H signals nevertheless appeared to be well behaved in this regard whilst the ^{13}C and ^{15}N signals were more capricious.

The chemical shifts changes for H-1, H-7, C-2, C-7 and N-1 all indicate that binding of $\mathbf{3_S}$ to **1** is occurring at the amide group, but there is also some evidence for binding to the imine N-10 nitrogen too in the presence of a large excess of $\mathbf{3_S}$ as it experiences a degree of shielding. Moreover, the most notable $\Delta\delta$s for enantioresolution are for H-7, H-11a, H-11b, C-2, C-3, C-4, C-4a, C-7, C-9, C-11, N-1 and N-10, thereby also implying a degree of binding to the imine N-10 nitrogen as well with regards to pertinent nuclei, and moreover, that the enantioresolution is very effective by this binding mode for the relevant nuclei. The two binding modes were also confirmed by NOE experiments. For example, amide-to-amide complexation was indicated by signal enhancements of both methyl groups of $\mathbf{3_S}$ upon irradiation of H-7 whilst amide-to-imine complexation was indicated by signal enhancement of the CH_3(CHOH) methyl group upon irradiation of H-4 and for irradiation of either H-11b or H-5, signal enhancements of both methyl groups and the methylene group. Since enantioresolution for **2** occurs in a similar manner to **1**, it implies that the predominant mechanism for enantioresolution for the spatially close nuclei to N-10 is by complexation of $\mathbf{3_S}$ to N-10, hence, quid pro quo. It is also notable that less of the CSA is required for enantioresolution of $\mathbf{2_{rac}}$ due to competing amide complexation in $\mathbf{1_{rac}}$. Interestingly, whilst enantioresolution is not evident for H-7 and C-7 in **2** – consistent with expectations since the NH proton has been replaced by a methoxy group – enantioresolution of H-13 and C-13, i.e. the nuclei of the methoxy group, occurs. However, whilst C-2 is enantioresolved, it is not significantly deshielded thereby not implying the occurrence of unexpected binding to the carbonyl oxygen O-2 and the enantioresolution of H-13 and C-13 remains a conundrum.

Although the enantioresolution of **1** and **2** using $\mathbf{3_S}$ was sufficient for analytical purposes in terms of quantification or identification of a known enantiomer, it had been hoped that determination of absolute configuration could be accessed via enantioresolved NMR signals in conjunction with modeling of the structures. Although the signal disparity between the enantiomers of **1** and **2** when complexed to $\mathbf{3_S}$ was not of the required manner for configuration determination with the approach in mind, nevertheless modeling of the two enantiomers of spirobrassinin ($\mathbf{1_R}$ and $\mathbf{1_S}$) complexed with $\mathbf{3_S}$ was undertaken. Correct enantiomeric assessment of the NMR signals for only a single or limited number of samples, whether it be for the identification of a known enantiomer or the determination of absolute configuration, requires both an evaluation of the relative strengths of the complexation as well as large relative $\Delta\delta$s [39]. However, with liberal dispersion between the signals for the complexed enantiomers, large $\Delta\delta$s from the free enantiomer per se are not completely necessary for the determination of absolute configuration [14,15,39].

Initial examinations at a lower level of theory {B3LYP/6-31G(d,p)} indicated monodentate binding of the hydroxyl group of $\mathbf{3_S}$ to the imine nitrogen N-10 of **1** to be several kcal/mol less stable in comparison to bidentate complexation by way of the hydroxyl group of $\mathbf{3_S}$ to the carbonyl oxygen O-2 of **1** and the carbonyl oxygen of $\mathbf{3_S}$ to the amide hydrogen H-1 of **1** (see Supplementary data). Thus, as occurred in the case of the dimeric complexes, dichotomy between experimental observation and the theoretical predictions was obtained and similar speculation regarding the likely cause(s) can be invoked. Nevertheless, examinations at the higher level only focused on bidentate complexation and example structures of the $\mathbf{1_S}$·$\mathbf{3_S}$ and $\mathbf{1_R}$·$\mathbf{3_S}$ complexes are depicted in Fig. 6 with the energies of the structures presented in Table 6. However, as mentioned above, experimentally there was evidence for a notable presence of imine bound complex in solution. This is akin

Table 5
^{13}C and ^{15}N NMR enantioresolution of the spirobrassinin enantiomers $\mathbf{1_R}$ and $\mathbf{1_S}$ and 1-methoxyspirobrassinin enantiomers $\mathbf{2_R}$ and $\mathbf{2_S}$ by complexation with $\mathbf{3_S}$.

Sample	[a]	C-2	C-3	C-4	C-4a	C-5	C-6	C-7	C-7a	C-9	C-11	C-12	C-13	Sample	[a]	N-1[b]	N-10[b]
$\mathbf{1_{rac}}$, dilute	δ (ppm)	177.45	65.04	124.57	131.35	123.27	129.35	110.06	140.22	163.27	75.21	15.28	–	Enrich. $\mathbf{1_R}$, conc.	δ (ppm)[c]	−247.99	−97.48
Enrich. $\mathbf{1_R}$, dilute + 59.1 equiv. $\mathbf{3_S}$	δ (ppm)[c]	178.14	65.28	124.54	131.78	123.31	129.57	110.12	140.91	163.52	75.21	15.33	–		$\Delta\delta$ (ppb)	−15.20	−44.65
	$\Delta\delta$ (ppb)	6.38	5.24	−4.78	6.83	–	4.10	11.16	2.96	−24.37	−3.19	–	–		$\Delta\nu$ (Hz)	−0.925	−2.717
	$\Delta\nu$ (Hz)	0.802	0.659	−0.601	0.859	–	0.515	1.461	0.372	−3.093	−0.401	–	–	Enrich. $\mathbf{1_R}$, dilute	δ (ppm)[c]	−249.99	−97.4
Enrich. $\mathbf{1_R}$, dilute	δ (ppm)[c]	178.39	65.26	124.49	131.71	123.30	129.59	110.78	140.98	163.51	75.09	15.33	–		$\Delta\delta$ (ppb)	−19.95	–
+ 59.1 equiv. $\mathbf{3_S}$[d]	$\Delta\delta$ (ppb)	10.02	7.06	−7.74	10.25	–	–	14.35	–	−35.53	−5.92	–	–		$\Delta\nu$ (Hz)	−1.214	–
	$\Delta\nu$ (Hz)	1.260	0.888	−0.974	1.289	–	–	1.804	–	−4.468	−0.687	–	–	Enrich. $\mathbf{1_R}$, conc. + 8.17 equiv. $\mathbf{3_S}$	δ (ppm)[c]	−246.45	-98.30
Enrich. $\mathbf{1_R}$, conc.	δ (ppm)[c]	178.56	65.35	124.49	131.62	123.36	129.66	110.86	140.97	163.61	75.15	15.35	–		$\Delta\delta$ (ppb)	32.30	21.38
+ 8.17 equiv. $\mathbf{3_S}$	$\Delta\delta$ (ppb)	3.42	5.92	−5.92	10.02	–	–	9.34	–	−24.37	–	–	–		$\Delta\nu$ (Hz)	1.965	1.300
	$\Delta\nu$ (Hz)	0.430	0.745	−0.745	1.260	–	–	1.174	–	−3.064	–	–	–	Enrich. $\mathbf{1_R}$, dilute + 8.17 equiv. $\mathbf{3_S}$	δ (ppm)	−248.91	−97.6
$\mathbf{2_{rac}}$, dilute	δ (ppm)	170.68	63.24	124.50	127.62	123.86	129.62	107.60	139.93	163.06	74.70	15.28	63.16	$\mathbf{2_{rac}}$, conc.	δ (ppm)[e]	−184.48	−97.33
$\mathbf{2_{rac}}$, dilute + 30.6 equiv. $\mathbf{3_S}$	δ (ppm)[e]	170.79	63.26	124.56	127.65	124.01	129.78	107.73	139.88	163.39	74.70	15.35	63.33	$\mathbf{2_{rac}}$, dilute	δ (ppm)[e]	−184.6	no
	$\Delta\delta$ (ppb)	7.29	–	–	–	–	–	–	–	12.75	–	–	5.24	$\mathbf{2_{rac}}$, conc. + 9.84 equiv. $\mathbf{3_S}$	δ (ppm)[e]	−184.34	−98.25
	$\Delta\nu$ (Hz)	0.916	–	–	–	–	–	–	–	1.604	–	–	0.659		$\Delta\delta$ (ppb)	–	18.05
$\mathbf{2_{rac}}$, conc. + 9.84 equiv. $\mathbf{3_S}$	δ (ppm)[e]	170.78	63.25	124.55	127.61	124.01	129.79	107.74	139.86	163.39	74.69	15.35	63.34		$\Delta\nu$ (Hz)	–	1.098
	$\Delta\delta$ (ppb)	7.06	–	–	–	–	–	–	–	12.53	–	–	4.78	$\mathbf{2_{rac}}$, dilute	δ (ppm)[e]	−184.9	no
	$\Delta\nu$ (Hz)	0.888	–	–	–	–	–	–	–	1.575	–	–	0.601	+ 9.84 equiv. $\mathbf{3_S}$			
$\mathbf{1_R}$·$\mathbf{3_S}$ − $\mathbf{1_R}$[f] (calculated[g])	$\Delta\delta$ (ppm)	−4.79	−1.45	0.63	−0.15	0.05	0.02	−1.70	−0.96	−0.41	0.38	−0.05	–	$\mathbf{1_R}$·$\mathbf{3_S}$ − $\mathbf{1_R}$[f] (calculated[g])	$\Delta\delta$ (ppm)	−10.07	0.33
$\mathbf{1_S}$·$\mathbf{3_S}$ − $\mathbf{1_R}$·$\mathbf{3_S}$[f] (calculated[g])	$\Delta\delta$ (ppm)	0.25	0.25	−0.01	−0.09	0.05	0.02	0.18	−0.12	0.11	−0.15	0.06	–	$\mathbf{1_S}$·$\mathbf{3_S}$ − $\mathbf{1_R}$·$\mathbf{3_S}$[f] (calculated[g])	$\Delta\delta$ (ppm)	0.19	0.03

no: not observed.
[a] The quantities $\Delta\delta$ and $\Delta\nu$ are the differences {value for the (*R*)-enantiomer – value for the (*S*)-enantiomer when known} between the signals of the two enantiomers in ppm and frequency, respectively.
[b] Shifts reported to two decimal places are taken from direct measurements; shifts reported to one decimal place are taken from indirect measurements.
[c] Chemical shifts of the signals of the (*R*)-enantiomer $\mathbf{1_R}$.
[d] Spectrum acquired at 8 °C.
[e] Enantiomers not identified.
[f] Difference of the shieldings, therefore negative values indicate that the former spin is deshielded relative to the latter.
[g] By DFT at the B3LYP/TZVP//B3LYP/cc-pVTZ level of theory using the GIAO method with solvation by benzene simulated by IEF-PCM using the uahf atomic radii set.

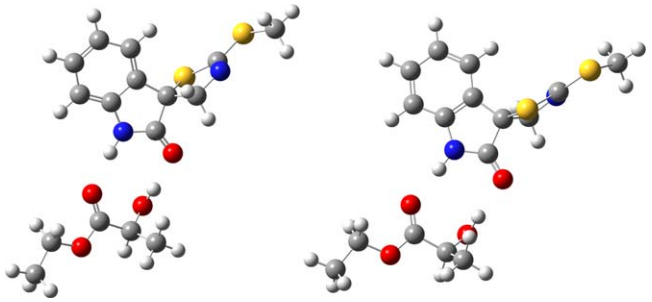

Fig. 6. The geometry-optimized structures of the complexes $\mathbf{1_S}\cdot\mathbf{3_S}$ (left) and $\mathbf{1_R}\cdot\mathbf{3_S}$ (right) at the B3LYP/TZVP (IEF-PCM) level of theory in benzene.

to the anomalies obtained for dimeric self-association and the same explanations can be invoked. Nonetheless, the energies do give a strong indication for the likelihood of resolution by the use of $\mathbf{3_S}$, and more so with the calculation of the NMR chemical shifts.

For the TZVP-optimized structures, chemical shieldings of complexes $\mathbf{1_R}\cdot\mathbf{3_S}$ and $\mathbf{1_S}\cdot\mathbf{3_S}$ were calculated by DFT at the B3LYP/TZVP//B3LYP/cc-pVTZ level of theory using the GIAO method with solvation by benzene simulated by IEF-PCM using the uahf atomic radii set and the results are included in Tables 4 and 5 for the ^{1}H, ^{13}C and ^{15}N nuclei as $\Delta\delta$s of the complexed (*R*)-enantiomer from the free enantiomer ($\mathbf{1_R}\cdot\mathbf{3_S}$–$\mathbf{1_R}$) and $\Delta\delta$s between the two complexed enantiomers ($\mathbf{1_S}\cdot\mathbf{3_S}$–$\mathbf{1_R}\cdot\mathbf{3_S}$). Qualitatively, good agreement was obtained for the complexed molecule relative to the free molecule for the nuclei involved with or close to the site of complexation, viz. H-1, H-7, C-2, C-7 and N-1, thereby substantiating the main mode of complexation. For comparison of the diastereomeric complexes, a significant number of the calculated $\Delta\delta$s were qualitatively in agreement with the observed $\Delta\delta$s. However, the experimental $\Delta\delta$s, though applicable for the identification of an enantiomer with an available authentic sample (and indeed, useful for quantitative purposes), were too small to be applied for the reliable identification of an enantiomer in the converse case by comparison to calculated values. Moreover, only for H-1 could resolution be anticipated, though this signal was not experimentally enantioresolved due to excessive line broadening masking any such occurrence.

Attempts made to chromatographically resolve racemic (±)-spirobrassinin ($\mathbf{1_{rac}}$) and racemic (±)-1-methoxyspirobrassinin ($\mathbf{2_{rac}}$) using TLC plates pre-treated with $\mathbf{3_S}$, a strategy that has worked for enantiomeric resolution previously [15], were unsuccessful for both compounds for a variety of conditions. Thus, the likely optimistic indications of resolution for **1** derived from the energies listed in Table 6, wherein the (*R*)-enantiomer $\mathbf{1_R}$ was anticipated to be retained relative to the (*S*)-enantiomer $\mathbf{1_S}$ based on the greater stabilization of the $\mathbf{1_R}\cdot\mathbf{3_S}$ complex upon changing to polar conditions and the greater overall stabilization of the $\mathbf{1_S}\cdot\mathbf{3_S}$ complex which is likely to permit faster passage of the (*S*)-enantiomer $\mathbf{1_S}$ due to lower impedance, did not materialize. Other attempts to effect chromatographic-type separation of racemic (±)-spirobrassinin ($\mathbf{1_{rac}}$) using $\mathbf{3_S}$ included both the addition of silica gel to an NMR sample ("TLC in an NMR tube") and "panning". For both methods, unequivocal results were not forthcoming though in both cases there appeared to be some small, albeit ever so slight, alteration in the enantiomeric composition in favor of the (*R*)-enantiomer $\mathbf{1_R}$, i.e. in the former case the (*R*)-enantiomer $\mathbf{1_R}$ was retained more in solution whilst in the latter method the amount present increased proportionally with progression of the process. These observations conflict with prediction but the situation is compounded by ESDAC which favors enrichment of the excess enantiomer, i.e. the (*R*)-enantiomer $\mathbf{1_R}$, under these conditions.

Table 6
DFT-calculated electronic and Gibbs' free energies of the complexes of spirobrassinin enantiomers $\mathbf{1_R}$ and $\mathbf{1_S}$ with $\mathbf{3_S}$ at the B3LYP/TZVP (IEF-PCM) level of theory.

Structure	Solvent	ΔE (kcal/mol)	ΔG (kcal/mol)	Hydrogen bonds, *r* (Å)	
				O–H···O=C	C=O···H–N
$\mathbf{1_S}\cdot\mathbf{3_S}$	Benzene	0.00	0.00	1.862	1.865
$\mathbf{1_R}\cdot\mathbf{3_S}$	Benzene	0.23	0.80	1.847	1.885
$\mathbf{1_S}\cdot\mathbf{3_S}$	Water	0.01	0.00	1.854	1.876
$\mathbf{1_R}\cdot\mathbf{3_S}$	Water	0.24	0.16	1.851	1.887

Acknowledgements

The Slovak Grant Agency for Science (Grant No. 1/3553/06), the Centre for International Mobility (grant to M.B.) and Turun Yliopistosäätiö are thanked for financial support. We also acknowledge the Center for Scientific Computing for computational resources and technical support.

Appendix A. Supplementary data

Supplementary data associated with this article can be found, in the online version, at doi:10.1016/j.jfluchem.2009.10.018.

References

[1] R.A. Dixon, C. Lamb, J. Ann. Rev. Plant Physiol. Plant Mol. Biol. 41 (1990) 339–367.
[2] T. Rouxel, A. Kollman, M.H. Belesdent, in: M. Daniel, R.P. Purkayastha (Eds.), Handbook of Phytoalexin Metabolism and Action, Marcel Dekker, New York, 1995, pp. 229–261.
[3] M.S.C. Pedras, F.I. Okanga, I.L. Zaharia, A.Q. Khan, Phytochemistry 53 (2000) 161–176.
[4] R.G. Mehta, J. Liu, A. Constantinou, M. Hawthorne, J.M. Pezzuto, R.C. Moon, R.M. Moriarty, Anticancer Res. 14 (1994) 1209–1214.
[5] R.G. Mehta, J. Liu, A. Constantinou, C.F. Thomas, M. Hawthorne, M. You, C. Gerhauser, J.M. Pezzuto, R.C. Moon, R.M. Moriarty, Carcinogenesis 16 (1995) 399–404.
[6] M. Sabol, P. Kutschy, L. Siegfried, A. Miroššay, M. Suchý, H. Hrbková, M. Dzurilla, R. Marušková, J. Starková, E. Paulíková, Biologia 55 (2000) 701–707.
[7] C.J. Moody, J.R.A. Roffey, M.A. Stephens, I.J. Stradford, Anti-Cancer Drugs 8 (1997) 489–499.
[8] M. Pilátová, M. Sarišský, P. Kutschy, A. Miroššay, R. Mezencev, Z. Čurillová, M. Suchý, K. Monde, L. Miroššay, J. Mojžiš, Leuk. Res. 29 (2005) 415–421.
[9] R. Mezencev, J. Mojžiš, M. Pilátová, P. Kutschy, Neoplasma 50 (2003) 239–245.
[10] R. Crossley, Chirality and the Biological Activity of Drugs, CRC Press, Boca Raton, FL, 1995.
[11] The recommendation of R.E. Gawley, J. Org. Chem. 71 (2006) 2411–2416 is followed with regards to the preferential use of enantiomer % over enantiomeric excess (e.e.).
[12] (a) H.Y. Aboul-Enein, I. Ali, Chiral Separations by Liquid Chromatography and Related Technologies, Marcel Dekker, New York, 2003;
(b) G. Subramanian (Ed.), Chiral Separation Techniques: A Practical Approach, third ed., Wiley–VCH, Weinheim, 2007.
[13] (a) W.H. Pirkle, D.J. Hoover, Top. Stereochem. 13 (1982) 263–331;
(b) T.J. Wenzel, J.D. Wilcox, Chirality 15 (2003) 256–270;
(c) D. Parker, Chem. Rev. 91 (1991) 1441–1457;
(d) T.J. Wenzel, Discrimination of Chiral Compounds Using NMR Spectroscopy, Wiley–VCH, Weinheim, 2007.
[14] V. Nieminen, D.Yu. Murzin, K.D. Klika, Org. Biomol. Chem. 7 (2009) 537–542.
[15] K.D. Klika, unpublished results.
[16] (a) V.A. Soloshonok, Angew. Chem. Int. Ed. 45 (2006) 766–769, and 13 other original references cited therein concerning the ESDAC phenomenon;
(b) R. Stephani, V.J. Cesare, J. Chromatogr. A 813 (1998) 79–84;
(c) R.M. Carman, K.D. Klika, Aust. J. Chem. 44 (1991) 895–896;
(d) V.A. Soloshonok, D.O. Berbasov, J. Fluor. Chem. 127 (2006) 597–603.
[17] (a) A review of the phenomenon is given by J. Martens, R. Bhushan, J. Liq. Chromatogr. Relat. Technol. 15 (1992) 1–27.;
(b) Reference [14] provides a listing of 8 references treating the topic.
(c) V.A. Soloshonok, D.O. Berbasov, Chim. Oggi-Chem. Today 24 (2006) 44–47.
[18] M. Takasugi, K. Monde, N. Katsui, A. Shirata, Chem. Lett. (1987) 1631–1632.
[19] M. Suchý, P. Kutschy, K. Monde, H. Goto, N. Harada, M. Takasugi, M. Dzurilla, E. Balentová, J. Org. Chem. 66 (2001) 3940–3947.
[20] D. Gross, A. Porzel, J. Schmidt, Z. Naturforsch. (C) 49 (1994) 281–285.
[21] P. Kutschy, M. Suchý, K. Monde, N. Harada, R. Marušková, Z. Čurillová, M. Dzurilla, M. Miklošová, R. Mezencev, J. Mojžiš, Tetrahedron Lett. 43 (2002) 9489–9492.

[22] Z. Čurillová, P. Kutschy, M. Budovská, A. Nakahashi, K. Monde, Tetrahedron Lett. 48 (2007) 8200–8204.
[23] K. Monde, T. Taniguchi, N. Miura, P. Kutschy, Z. Čurillová, M. Pilátová, J. Mojžiš, Bioorg. Med. Chem. 13 (2005) 5206–5212.
[24] M.S.C. Pedras, M. Hossain, M.G. Sarwar, S. Montaut, Bioorg. Med. Chem. Lett. 14 (2004) 5469–5471.
[25] K.D. Klika, M. Kramer, E. Kleinpeter, Theochem. J. Mol. Struct. 913 (2009) 247–253.
[26] (a) J. Stonehouse, P. Adell, J. Keeler, A.J. Shaka, J. Am. Chem. Soc. 116 (1994) 6037–6038;
(b) K. Stott, J. Stonehouse, J. Keeler, T.L. Hwang, A.J. Shaka, J. Am. Chem. Soc. 117 (1995) 4199–4200.
[27] (a) P. Virta, A. Koch, M.U. Roslund, P. Mattjus, E. Kleinpeter, L. Kronberg, R. Sjöholm, K.D. Klika, Org. Biomol. Chem. 3 (2005) 2924–2929;
(b) E. Balentová, J. Imrich, J. Bernát, L. Suchá, M. Vilková, N. Prónayová, P. Kristian, K. Pihlaja, K.D. Klika, J. Heterocycl. Chem. 43 (2006) 645–656;
(c) Z. Fröhlichová, J. Imrich, I. Danihel, P. Kristian, S. Böhm, D. Sabolová, M. Kožurková, O. Hritzová, B. Horváth, T. Bušová, K.D. Klika, Spectroc. Acta Pt. A 73 (2009) 238–248.
[28] J. Mäki, P. Tähtinen, L. Kronberg, K.D. Klika, J. Phys. Org. Chem. 18 (2005) 240–249.
[29] See for example: R. Laatikainen, M. Niemitz, U. Weber, J. Sundelin, T. Hassinen, J. Vepsäläinen, J. Magn. Reson. Ser. A 120 (1996) 1–10; see also: Peak Research NMR Software, Perch Solutions Ltd., Kuopio, Finland, 2003 (http://www.perchsolutions.com).
[30] A.D. Becke, J. Chem. Phys. 98 (1993) 5648–5652.
[31] M.J. Frisch, G.W. Trucks, H.B. Schlegel, G.E. Scuseria, M.A. Robb, J.R. Cheeseman, J.A. Montgomery Jr., T. Vreven, K.N. Kudin, J.C. Burant, J.M. Millam, S.S. Iyengar, J. Tomasi, V. Barone, B. Mennucci, M. Cossi, G. Scalmani, N. Rega, G.A. Petersson, H. Nakatsuji, M. Hada, M. Ehara, K. Toyota, R. Fukuda, J. Hasegawa, M. Ishida, T. Nakajima, Y. Honda, O. Kitao, H. Nakai, M. Klene, X. Li, J.E. Knox, H.P. Hratchian, J.B. Cross, V. Bakken, C. Adamo, J. Jaramillo, R. Gomperts, R.E. Stratmann, O. Yazyev, A.J. Austin, R. Cammi, C. Pomelli, J.W. Ochterski, P.Y. Ayala, K. Morokuma, G.A. Voth, P. Salvador, J.J. Dannenberg, V.G. Zakrzewski, S. Dapprich, A.D. Daniels, M.C. Strain, O. Farkas, D.K. Malick, A.D. Rabuck, K. Raghavachari, J.B. Foresman, J.V. Ortiz, Q. Cui, A.G. Baboul, S. Clifford, J. Cioslowski, B.B. Stefanov, G. Liu, A. Liashenko, P. Piskorz, I. Komaromi, R.L. Martin, D.J. Fox, T. Keith, M.A. Al-Laham, C.Y. Peng, A. Nanayakkara, M. Challacombe, P.M.W. Gill, B. Johnson, W. Chen, M.W. Wong, C. Gonzalez, J.A. Pople, Gaussian03, Revision D. 02, Gaussian, Inc., Wallingford, CT, 2003.
[32] (a) A.D. Becke, Phys. Rev. A 38 (1988) 3098–3100;
(b) C. Lee, W. Yang, R.G. Parr, Phys. Rev. B 37 (1988) 785–789;
(c) B. Miehlich, A. Savin, H. Stoll, H. Preuss, Chem. Phys. Lett. 157 (1989) 200–206.
[33] A.P. Scott, L. Radom, J. Phys. Chem. 100 (1996) 16502–16513.
[34] K. Wolinski, J.F. Hinton, P. Pulay, J. Am. Chem. Soc. 112 (1990) 8251–8260.
[35] And also accepting that the slight splitting observed on a few signals would not be evident with typical acquisition conditions and parameters with regards to field homogeneity (“shim”), acquired resolution and processing.
[36] (a) J. Mäki, K.D. Klika, R. Sjöholm, L. Kronberg, J. Chem. Soc., Perkin Trans. 1 (2001) 1216–1219;
(b) M. Alei, L.O. Morgan, W.E. Wagerman, T.M. Whaley, J. Am. Chem. Soc. 102 (1980) 2881–2887.
[37] A. Bagno, G. Scorrano, Acc. Chem. Res. 33 (2000) 609–616.
[38] (a) K.D. Klika, E. Balentová, J. Bernát, J. Imrich, M. Vavrušová, E. Kleinpeter, K. Pihlaja, A. Koch, J. Heterocycl. Chem. 43 (2006) 633–643;
(b) K.D. Klika, E. Balentová, J. Bernát, J. Imrich, M. Vavrušová, K. Pihlaja, A. Koch, E. Kleinpeter, A. Kelling, U. Schilde, ARKIVOC xvi (2006) 93–108;
(c) S. Böhm, J. Tomaščiková, J. Imrich, I. Danihel, P. Kristian, A. Koch, E. Kleinpeter, K.D. Klika, Theochem. J. Mol. Struct. 916 (2009) 105–118.
[39] K.D. Klika, Tetrahedron Asym. 20 (2009) 1099–1102.